Critical behavior of the quasi-two-dimensional weak itinerant ferromagnet trigonal chromium telluride $Cr_{0.62}Te$

Yu Liu (刘育) and C. Petrovic

Condensed Matter Physics and Materials Science Department, Brookhaven National Laboratory, Upton, New York 11973, USA

(Received 24 July 2017; revised manuscript received 20 September 2017; published 9 October 2017; corrected 29 November 2018 and 14 January 2020)

The critical properties of flux-grown single-crystalline quasi-two-dimensional weak itinerant ferromagnet $Cr_{0.62}Te$ were investigated by bulk dc magnetization around the paramagnetic to ferromagnetic phase transition. Critical exponents $\beta = 0.315(7)$ with a critical temperature $T_c = 230.6(3)$ K and $\gamma = 1.81(2)$ with $T_c = 229.1(1)$ K are obtained by the Kouvel-Fisher method whereas $\delta = 6.35(4)$ is obtained by a critical isotherm analysis at $T_c = 230$ K. With these obtained exponents, the magnetization-field-temperature curves collapse into two independent curves following a single scaling equation $M|\frac{T-T_c}{T_c}|^{-\beta} = f_{\pm}(H|\frac{T-T_c}{T_c}|^{-\beta\delta})$ around T_c, suggesting the reliability of the obtained exponents. Additionally, the determined exponents of $Cr_{0.62}Te$ exhibit an Ising-like behavior with a change from short-range order to long-range order in the nature of magnetic interaction and with an extension from two to three dimensions on cooling through T_c.

DOI: 10.1103/PhysRevB.96.134410

I. INTRODUCTION

Two-dimensional (2D) materials such as graphene and ultrathin transition-metal dichalcogenides have been attracting significant interest due to their highly tunable physical properties and immense potential in scalable device applications [1–4]. However, in contrast to mechanical and optoelectronic properties, the investigation of magnetism in 2D materials has received little attention. Recently, the Cr chalcogenides are of great interest for possible application in spintronic technologies. The $CrXTe_3$ (X = Si, Ge, Sn) have been identified as promising candidates for long-range magnetism in monolayer [5–7]. $CrSiTe_3$ exhibits ferromagnetic (FM) ordering at ∼32 K in the bulk [8], and it can be enhanced to ∼80 K in monolayer and few-layer samples [9]. Bulk $CrGeTe_3$ are ferromagnetic at ∼61 K, which is still somewhat low for spintronic applications [10].

In the binary Cr-based chalcogenides, tellurides CrTe, Cr_3Te_4, Cr_2Te_3, Cr_5Te_8 are ferromagnetic with metallic conductivity [11–17], while selenides CrSe, Cr_3Se_4, Cr_2Se_3, Cr_5Se_8 and sulfides CrS, Cr_5S_6, Cr_3S_4, Cr_2S_3, Cr_5S_8 are predominantly antiferromagnetic (AFM) showing either metallic or semiconducting behavior [18–22]. Among these compounds, the $Cr_{1-x}Te$ system shows ferromagnetism with T_c of 170 ∼ 360 K [11]. $Cr_{1-x}Te$ with $x < 0.1$ crystallize in the hexagonal NiAs structure, while Cr_3Te_4 ($x = 0.25$) and Cr_2Te_3 ($x = 0.33$) form monoclinic and trigonal crystal structures where Cr vacancies occupy in every second metal layer. According to neutron-diffraction studies, the saturation magnetization in this system is small and it could be partly explained if spin canting is taken into consideration for x = 0.125, 0.167, and 0.25 [23]. The magnetic moment induced on the Cr ion for $x = 0.25$ is close to an integral number of Bohr magnetons, suggesting the existence of mixed valence Cr [23]. However, for Cr_2Te_3 ($x = 0.33$), the ordered magnetic moment of 2.65–2.70μ_B deduced from the neutron diffraction is much smaller than that calculated using the ionic model $3\mu_B$, suggesting the itinerant nature of the d electrons [13,23]. The electron correlation effects in itinerant ferromagnets has also been discussed in the photoemission spectra [24]. Until now, only a few studies were performed on $Cr_{1-x}Te$ with $x = 0.375$, of which the trigonal phase exhibits a higher T_c than that of the monoclinic phase [15].

Trigonal $Cr_{0.62}Te$ exhibits weak itinerant ferromagnetic character with $T_c \approx 237$ K. In order to understand the nature of the FM transition, we investigated its critical behavior by modified Arrott plot, Kouvel-Fisher plot, and critical isotherm analysis. The determined exponents $\beta = 0.315(7)$ with $T_c = 230.65(26)$ K, $\gamma = 1.81(2)$ with $T_c = 229.11(5)$ K, and $\delta = 6.35(4)$ at $T_c = 230$ K indicate a change in the nature of magnetic interaction passing from short-range order to long-range order with an extension from two to three dimensions on cooling through T_c.

II. EXPERIMENTAL DETAILS

The trigonal $Cr_{0.62}Te$ single crystals were grown by the self-flux technique starting from an intimate mixture of pure elements Cr (99.99%, Alfa Aesar) powder and Te (99.9999%, Alfa Aesar) pieces with a molar ratio of 0.06 : 0.94. Starting materials were sealed in an evacuated quartz tube, which was heated to 900 °C over 20 h, held at 900 °C for 3 h, and then slowly cooled to 500 °C at a rate of 1 °C/h. X-ray diffraction (XRD) data were taken with Cu K_α ($\lambda = 0.15418$ nm) radiation of Rigaku Miniflex powder diffractometer. The element analysis was performed using an energy-dispersive x-ray spectroscopy (EDX) in a JEOL LSM-6500 scanning electron microscope, confirming a near-stoichiometric $Cr_{0.62}Te$ single crystal. The magnetization was measured in a Quantum Design magnetic property measurement system (MPMS-XL5). The isothermal $M(H)$ curves are measured in $\Delta T = 1$ K intervals. The applied magnetic field (H_a) has been corrected for the internal field as $H = H_a - NM$, where M is the measured magnetization and N is the demagnetization factor. The corrected H was used for the analysis of critical behavior.

III. RESULTS AND DISCUSSIONS

The Cr-Te phase diagram was summarized by Herbert *et al.* [11]. The multiple $Cr_{1-x}Te$ phases with structures

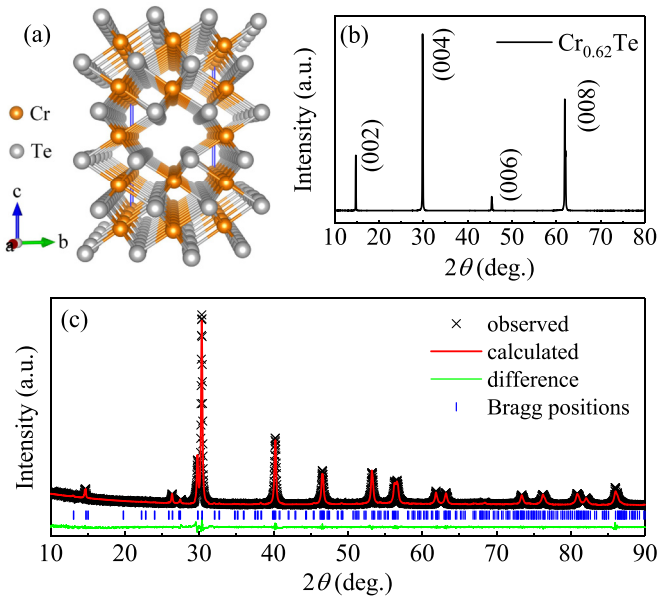

FIG. 1. (a) Crystal structure of $Cr_{0.62}Te$. (b) Single-crystal x-ray diffraction (XRD) and (c) powder XRD pattern of $Cr_{0.62}Te$. The vertical tick marks represent Bragg reflections of the $P\bar{3}m1$ space group.

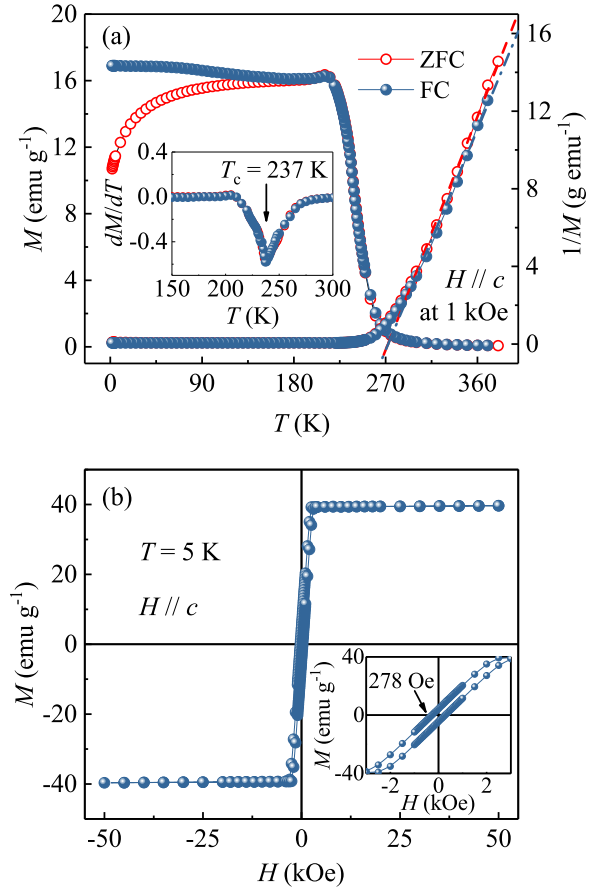

FIG. 2. (a) Temperature dependence of magnetization for $Cr_{0.62}Te$ measured in the external magnetic field $H = 1$ kOe applied along the c axis with zero-field-cooling (ZFC) and field-cooling (FC) modes. The dashed lines are fits by the modified Curie-Weiss law $\chi = \frac{C}{T-\theta} + \chi_0$, where χ_0 is the temperature-independent susceptibility, C is the Curie-Weiss constant, and θ is the Weiss temperature. Inset: the derivative magnetization dM/dT vs T. (b) Field dependence of magnetization for $Cr_{0.62}Te$ measured at $T = 5$ K. Inset: the magnification of the low-field region.

intermediate between the NiAs and the CdI_2 types depend on the different arrangements of metal atom vacancies. So far, the trigonal $Cr_{0.62}Te$ in which the Cr atoms are located on four crystallographically different sites leading to the formation of a five-layer superstructure of the CdI_2 type [Fig. 1(a)] has been rarely studied [25]. In the CdI_2-type structure the second basal planes for Cr atoms of NiAs-type structure are partially occupied by Cr vacancies and the Cr atoms are surrounded by the octahedral environment of Te anions [15]. Figure 1(b) presents the single-crystal x-ray diffraction (XRD) pattern of $Cr_{0.62}Te$. Only $(00l)$ peaks are detected, indicating the crystal surface is normal to the c axis with the plate-shaped surface parallel to the ab plane. As shown in Fig. 1(c), the powder XRD pattern is well fitted with the $P\bar{3}m1$ space group. The determined lattice parameters $a = 0.7792(2)$ nm and $c = 1.1980(2)$ nm are very close to the values in a previous report [15].

Figure 2(a) shows the temperature dependence of magnetization $M(T)$ measured in $H = 1$ kOe applied parallel to the c axis, in which a clear paramagnetic (PM) to ferromagnetic (FM) transition is observed. As shown in the inset in Fig. 2(a), the critical temperature $T_c \approx 237$ K is roughly determined from the minimum of the derivative dM/dT curve, which is in good agreement with the value reported previously [15]. The zero-field-cooling (ZFC) and field-cooling (FC) curves show significant splitting at low temperatures, indicating a strong magnetocrystalline anisotropy or spin canting. The $1/M$ vs T is also plotted in Fig. 2(a). A linear fit in the high-temperature range of $290 \sim 350$ K yields the Weiss temperature $\theta = 272(1)$ K, indicating predominant FM exchange interaction. The deduced effective moment $\mu_{\text{eff}} = 3.93(3)\mu_B$/Cr for the ZFC curve is close to $\mu_{\text{eff}} = 4.04(5)\mu_B$/Cr for the FC data, in agreement with the theoretical value expected for Cr^{3+} of $3.87\mu_B$. Figure 2(b) displays the isothermal magnetization measured at $T = 5$ K. The saturation field is $H_s \approx 3$ kOe and the saturation moment at $T = 5$ K is $M_s \approx 1.814(1)\mu_B$/Cr. The inset in Fig. 2(b) shows the $M(H)$ in the low-field region and little hysteresis with the coercive force $H_c = 278$ Oe. All these results are in good agreement with the previous report [15]. Then we calculated the Rhodes-Wohlfarth ratio (RWR) for $Cr_{0.62}Te$, which is defined as P_c/P_s with P_c obtained from the effective moment $P_c(P_c + 2) = P_{\text{eff}}^2$ and P_s is the saturation moment obtained in the ordered state [26,27]. RWR is 1 for localized systems and is larger in an itinerant system. Here we obtain RWR = 1.69 for ZFC and RWR = 1.74 for FC, indicating weak itinerant character of FM in $Cr_{0.62}Te$.

In order to understand the nature of the FM transition in $Cr_{0.62}Te$, one approach is to study in detail the critical exponents associated with the transition. Isothermal magnetization $M(H)$ around T_c was measured from $T = 220$ K to $T = 250$ K at intervals of 1 K to investigate the critical behavior, as shown in Fig. 3(a). Figure 3(b) presents the Arrott plot of M^2 vs H/M. Generally, M^2 vs H/M should be a series of parallel straight lines in the high-field range in the Arrott plot [28]. The intercept of the M^2 as a function

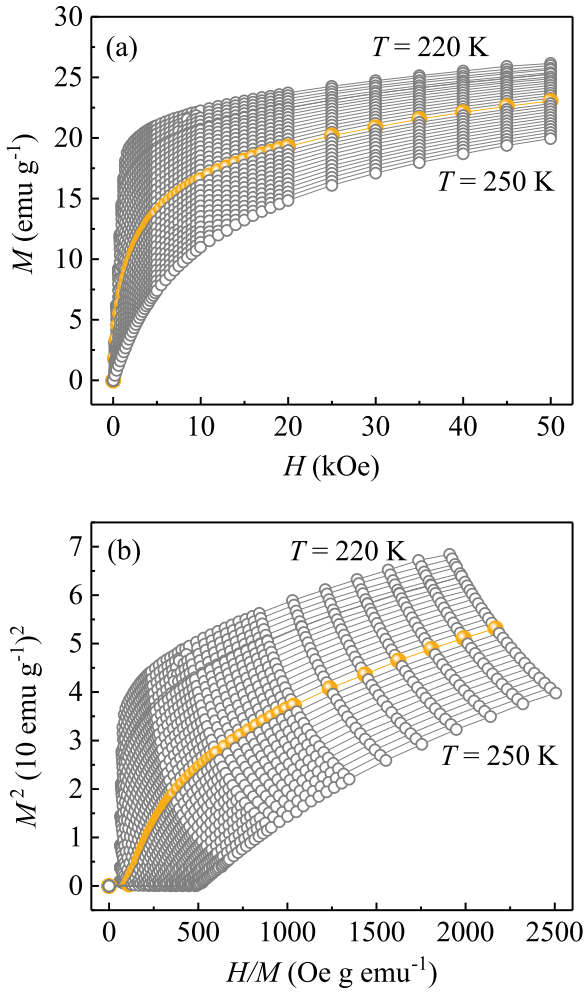

FIG. 3. (a) Typical initial isothermal magnetization curves measured along the c axis around $T_c = 237$ K (orange symbol and line) for $Cr_{0.62}Te$. (b) Arrott plots of M^2 vs H/M around T_c for $Cr_{0.62}Te$.

of H/M on the H/M axis is negative above T_c while it is positive below T_c. The line of M^2 vs H/M at T_c should pass through the origin. According to the criterion proposed by Banerjee [29], the order of the magnetic transition can be determined from the slope of the straight line: the positive slope corresponds to the second-order transition while the negative corresponds to the first-order one. Apparently, the positive slope of the M^2 vs H/M implies that the PM-FM transition in $Cr_{0.62}Te$ is a second-order one, as shown in Fig. 3(b). However, all the curves in this plot are nonlinear and show downward curvature even in the high-field region, which indicates that the long-range Landau mean-field theory with $\beta = 0.5$ and $\gamma = 1.0$ is not satisfied for $Cr_{0.62}Te$ according to Arrot-Noaks equation of state $(H/M)^{1/\gamma} = a\varepsilon + bM^{1/\beta}$, where $\varepsilon = (T - T_c)/T_c$ is the reduced temperature, and a and b are constants [30]. Hence, a modified Arrott plot should be used to obtain the critical parameters.

It is well known that for a second-order transition, its critical behavior can be characterized in detail by a series of interrelated critical exponents [31]. In the vicinity of a second-order phase transition, the divergence of correlation length $\xi = \xi_0|(T - T_c)/T_c|^{-\nu}$ leads to universal scaling laws for the spontaneous magnetization M_s and the inverse initial magnetic susceptibility χ_0^{-1}. The mathematical definitions of the exponents from magnetization can be described as

$$M_s(T) = M_0(-\varepsilon)^{\beta}, \quad \varepsilon < 0, \quad T < T_c, \tag{1}$$

$$\chi_0^{-1}(T) = (h_0/m_0)\varepsilon^{\gamma}, \quad \varepsilon > 0, \quad T > T_c, \tag{2}$$

$$M = DH^{1/\delta}, \quad \varepsilon = 0, \quad T = T_c, \tag{3}$$

where $\varepsilon = (T - T_c)/T_c$ is the reduced temperature, and M_0, h_0/m_0, and D are the critical amplitudes [31,32]. Parameters β (associated with M_s), γ (associated with χ_0), and δ (associated with T_c) are critical exponents. A 3D Heisenberg model ($\beta = 0.365, \gamma = 1.386$), a 3D XY model ($\beta = 0.345, \gamma = 1.316$), a 3D Ising model ($\beta = 0.325, \gamma = 1.24$), and a tricritical mean-field model ($\beta = 0.25, \gamma = 1.0$) are used to construct a modified Arrott plots [33], as given in Fig. 4. All these models yield quasistraight lines in the high-field region, however, the lines in Fig. 4(d) are not parallel to each other, indicating that the tricritical mean-field model is not satisfied. In order to distinguish which model is the best, normalized slopes (NS), which is defined as $\mathrm{NS} = S(T)/S(T_c)$ (where $S(T)$ is the slope of $M^{1/\beta}$ vs $(H/M)^{1/\gamma}$), are plotted in Fig. 5. In an ideal model, all values of NS should be equal to 1.0 because the modified Arrott plot should consist of a series of parallel straight lines. For $Cr_{0.62}Te$, the NS of a 3D Ising model is close to $\mathrm{NS} = 1$ mostly below T_c, while that of a 3D Heisenberg model is best above T_c, indicating that the critical behavior of $Cr_{0.62}Te$ may not belong to a single universality class.

In order to obtain the precise critical exponents β and γ, a rigorous iterative method has been used [34]. The linear extrapolation from the high-field region to the intercepts with the axis $M^{1/\beta}$ and $(H/M)^{1/\gamma}$ yields reliable values of $M_s(T)$ and $\chi_0^{-1}(T)$. A set of β and γ can be obtained by fitting data following Eqs. (1) and (2), which is used to reconstruct a new modified Arrott plot. Then, a new set of β and γ can be obtained. This procedure is repeated until the values of β and γ do not change. By this method, the obtained critical exponents do not depend on the initial parameters, which confirms that these critical exponents are reliable and intrinsic. Figure 6(a) presents the final $M_s(T)$ and $\chi_0^{-1}(T)$ with the solid fitting curves. The critical exponents $\beta = 0.314(7)$ with $T_c = 230.76(9)$ K and $\gamma = 1.83(2)$ with $T_c = 229.0(2)$ K are obtained. More accurately, the critical exponents can be determined according to the Kouvel-Fisher (KF) method [35]:

$$\frac{M_s(T)}{dM_s(T)/dT} = \frac{T - T_c}{\beta}, \tag{4}$$

$$\frac{\chi_0^{-1}(T)}{d\chi_0^{-1}(T)/dT} = \frac{T - T_c}{\gamma}. \tag{5}$$

According to the KF method, $M_s(T)/[dM_s(T)/dT]$ and $\chi_0^{-1}(T)/[d\chi_0^{-1}(T)/dT]$ are linear functions of temperature with slopes of $1/\beta$ and $1/\gamma$, respectively. As shown in Fig. 6(b), the linear fits give $\beta = 0.315(7)$ with $T_c = 230.6(3)$ K and $\gamma = 1.81(2)$ with $T_c = 229.1(1)$ K, respectively, which are consistent with those generated by the modified Arrott plot.

As confirmation, the critical exponents can be tested according to the prediction of the scaling hypothesis. In the critical asymptotic region, the magnetic equation can be

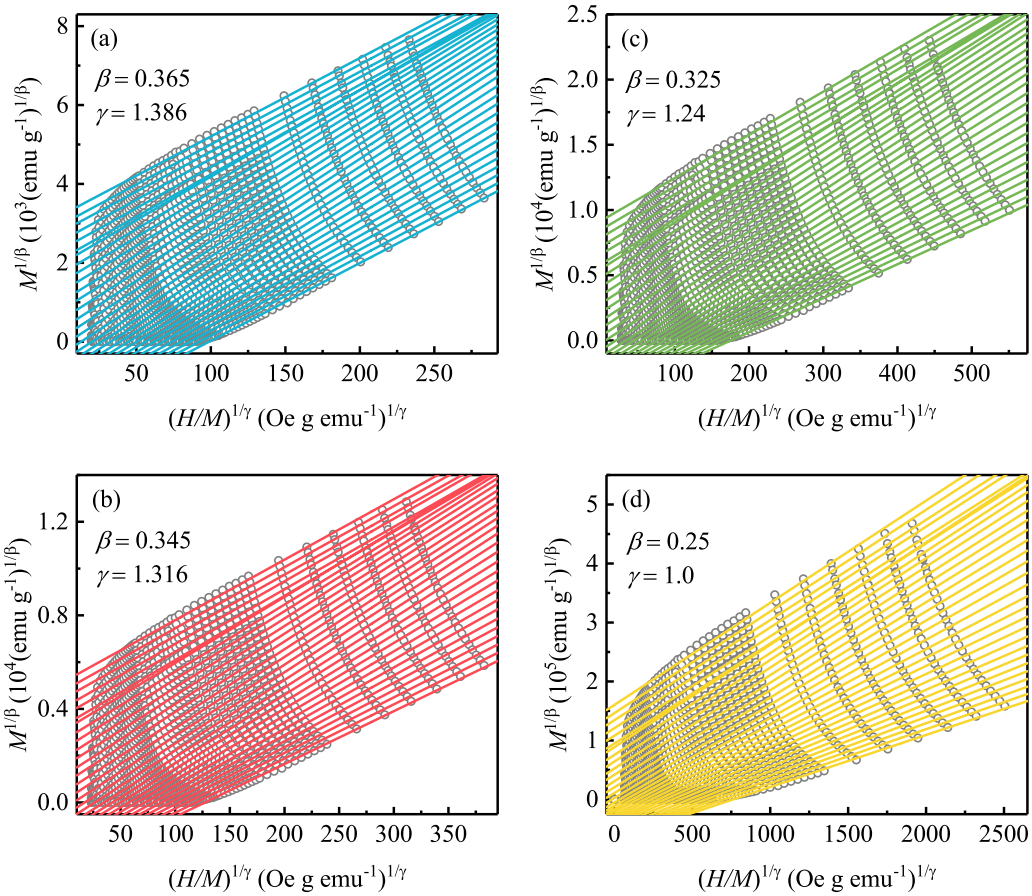

FIG. 4. The isotherms of $M^{1/\beta}$ vs $(H/M)^{1/\gamma}$ with parameters of (a) 3D Heisenberg model, (b) 3D XY model, (c) 3D Ising model, and (d) tricritical mean-field model. The straight lines are the linear fit of isotherms at different temperatures.

written as [31]

$$M(H,\varepsilon) = \varepsilon^{\beta} f_{\pm}(H/\varepsilon^{\beta+\gamma}), \tag{6}$$

where f_+ for $T > T_c$ and f_- for $T < T_c$, respectively, are the regular functions. In terms of renormalized magnetization $m \equiv \varepsilon^{-\beta} M(H,\varepsilon)$ and renormalized field $h \equiv \varepsilon^{-(\beta+\gamma)} H$, Eq. (6) can be written as

$$m = f_{\pm}(h); \tag{7}$$

it implies that for true scaling relations and the right choice of β, γ, and δ values, scaled m and h will fall on two universal curves: one above T_c and another below T_c. This is an important criterion for the critical regime. Following Eq. (7), scaled m vs scaled h has been plotted in Fig. 7(a), with the logarithmic scale in the inset of Fig. 7(a). It is rather significant that all the data collapse into two separate branches: one below T_c and another above T_c. The reliability of the exponents and T_c has been further ensured with more rigorous method by plotting m^2 vs h/m, as shown in Fig. 7(b), where all data also fall on two independent branches. This clearly indicates that the interactions get properly renormalized in critical regime following scaling equation of state. In addition, the scaling equation of state takes another form:

$$\frac{H}{M^{\delta}} = k\left(\frac{\varepsilon}{H^{1/\beta}}\right), \tag{8}$$

where $k(x)$ is the scaling function. Based on Eq. (8), all experimental curves will collapse into a single curve. The inset in Fig. 7(b) shows the $MH^{-1/\delta}$ vs $\varepsilon H^{-1/(\beta\delta)}$ for $Cr_{0.62}Te$, where the experimental data collapse into a single curve, and T_c locates at the zero point of the horizontal axis. The well-rescaled curves further confirm the reliability of the obtained critical exponents.

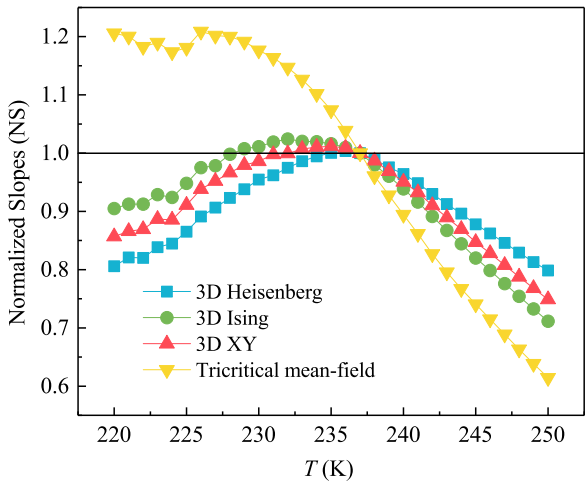

FIG. 5. Temperature dependence of the normalized slopes NS = $S(T)/S(T_c)$.

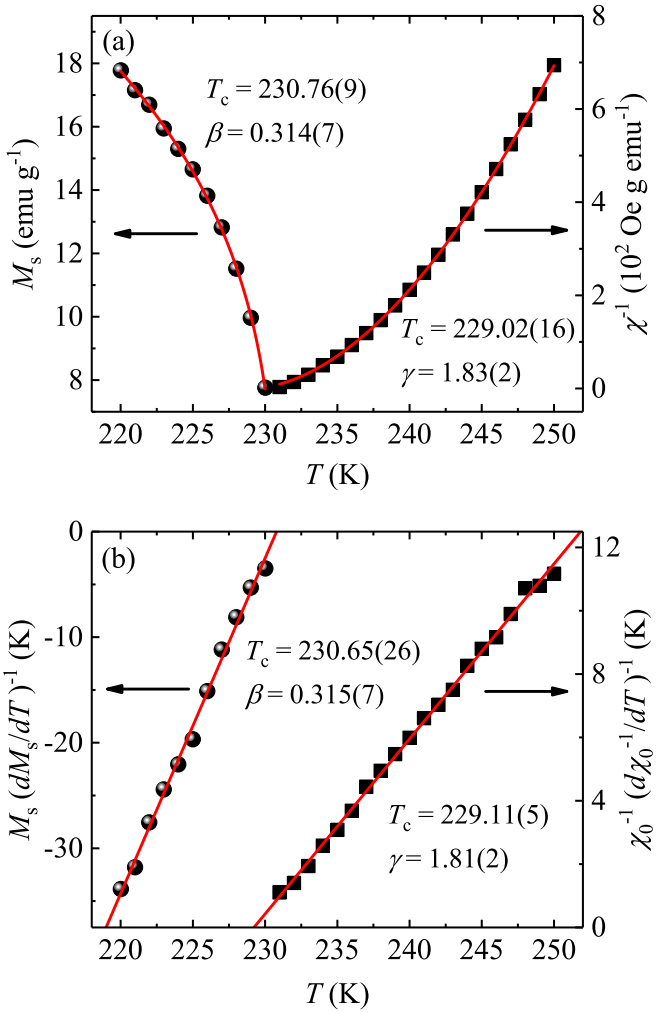

FIG. 6. (a) Temperature dependence of the spontaneous magnetization M_s (left) and the inverse initial susceptibility χ_0^{-1} (right) with solid fitting curves for $Cr_{0.62}Te$. (b) Kouvel-Fisher plots of $M_s(dM_s/dT)^{-1}$ (left) and $\chi_0^{-1}(d\chi_0^{-1}/dT)^{-1}$ (right) with solid fitting curves for $Cr_{0.62}Te$.

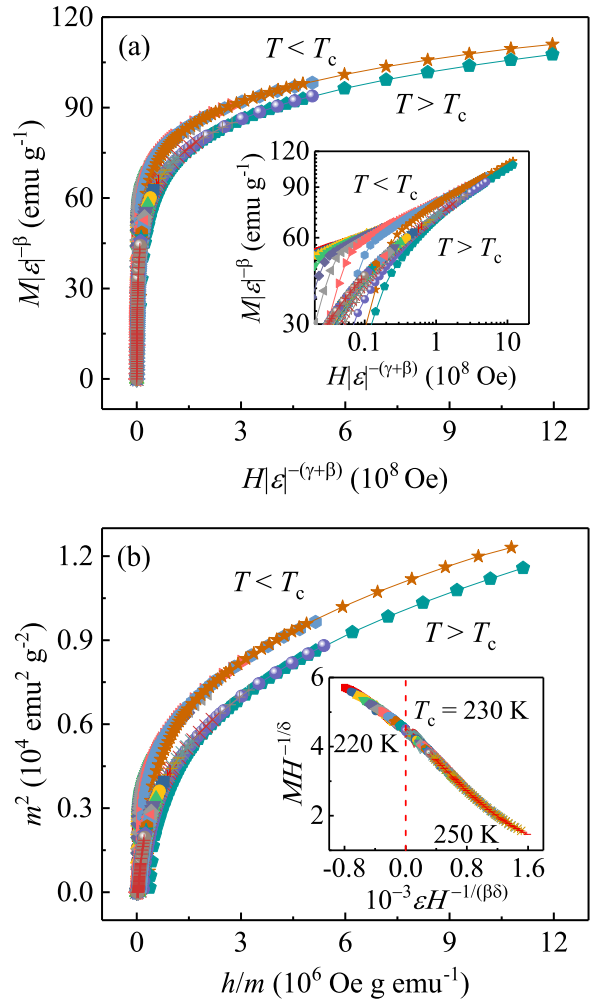

FIG. 7. (a) Scaling plots of renormalized magnetization m vs renormalized field h below and above T_c for $Cr_{0.62}Te$. Inset: the same plots in log-log scale. (b) Renormalized magnetization and field replotted in the form of m^2 vs h/m for $Cr_{0.62}Te$. Inset: the rescaling of the $M(H)$ curves by $MH^{-1/\delta}$ vs $\varepsilon H^{-1/(\beta\delta)}$.

The critical exponent δ can be determined by the critical isotherm analysis from $M(H)$ at T_c following Eq. (3). It is determined that $T_c = 230$ K from the obtained critical exponents. Thus, the isothermal magnetization $M(H)$ at $T_c = 230$ K is shown in Fig. 8, where the inset plots the logarithmic scale. The $\log(M)$-$\log(H)$ relation yields straight line at higher field range ($H > 3$ kOe) with the slope $1/\delta$, where $\delta = 6.35(4)$ is obtained. According to the statistical theory, these three critical exponents should agree with the Widom scaling relation [36]:

$$\delta = 1 + \frac{\gamma}{\beta}. \tag{9}$$

Using the β and γ values determined from the modified Arrott plot and Kouvel-Fisher plot, we obtain $\delta = 6.83(7)$ and $\delta = 6.75(6)$, respectively, which slightly deviates from that obtained from critical isotherm analysis $\delta = 6.35(4)$. The slight deviation from the Widom scaling law indicates that the critical behavior of $Cr_{0.62}Te$ does not belong to a single university class as a result of possible complex competition of several magnetic interactions.

The obtained critical exponents of $Cr_{0.62}Te$, as well as those of different theoretical models [37–39]. are listed in Table I for comparison. As we can see, the critical exponents of $Cr_{0.62}Te$ do not belong to any single universality class. For a homogeneous magnet, the universality class of the magnetic phase transition depends on the exchange distance $J(r)$. A renormalization-group theory analysis suggests that the long-range exchange interaction decays as $J(r) \sim r^{-(d+\sigma)}$, where d is the spatial dimension and σ is a positive constant, and the short-range exchange interaction decays as $J(r) \sim e^{-r/b}$, where b is the spatial scaling factor [32,37,40]. The long- or short-range of spin interaction depends on the value of σ, which is determined by [32,34,41]

$$\gamma = 1 + \frac{4}{d}\left(\frac{n+2}{n+8}\right)\Delta\sigma + \frac{8(n+2)(n-4)}{d^2(n+8)^2} \times \left[1 + \frac{2G(\frac{d}{2})(7n+20)}{(n-4)(n+8)}\right]\Delta\sigma^2, \tag{10}$$

TABLE I. Comparison of critical exponents of $Cr_{0.62}Te$ with different theoretical models.

Composition	Reference	Technique	T_c	β	γ	δ
$Cr_{0.62}Te$	this work	modified Arrott plot	230.76(9)	0.314(7)	1.83(2)	6.83(7)
	this work	Kouvel-Fisher plot	230.65(26)	0.315(7)	1.81(2)	6.75(6)
	this work	critical isotherm				6.35(4)
$\{d:n\}=\{2:1\}$						
2D short range $[J(r)\sim e^{-r/b}]$	37	theory		0.125	**1.75**	15.0
$\{d:n\}=\{2:1\}$						
2D long range $[J(r)\sim r^{-(d+\sigma)}]$	37	theory		**0.298**	1.393	5.67
$\{d:n\}=\{3:1\}$						
3D Ising model	38	theory		**0.325**	1.24	4.82
$\{d:n\}=\{3:2\}$						
3D XY model	38	theory		0.345	1.316	4.81
$\{d:n\}=\{3:3\}$						
3D Heisenberg model	38	theory		0.365	1.386	4.8
Mean-field model	38	theory		0.5	1.0	3.0
Tricritical mean field	39	theory		0.25	1.0	5.0

where $\Delta\sigma=(\sigma-\frac{d}{2})$ and $G(\frac{d}{2})=3-\frac{1}{4}(\frac{d}{2})^2$, n is the spin dimensionality. The short-range Heisenberg model is valid when $\sigma>2$, while the long-range mean-field model is satisfied when $\sigma<3/2$. In the present case, based on the experimental $\gamma=1.81(2)$, it can be obtained that $\sigma=1.626$ following Eq. (10). It can be seen that σ lies between the long-range and short-range interaction ($3/2<\sigma<2$). In addition, one can see that $\gamma=1.81(2)$ is close to the short-range interaction with $\{d:n\}=\{2:1\}$ ($\beta=0.125$, $\gamma=1.75$, and $\delta=15.0$), however, $\beta=0.315(7)$ approaches the long-range interaction with $\{d:n\}=\{2:1\}$ ($\beta=0.298$, $\gamma=1.392$, and $\delta=5.67$) and/or 3D Ising model with $\{d:n\}=\{3:1\}$ ($\beta=0.325$, $\gamma=1.24$, and $\delta=4.82$) (as listed in Table I). The previous photoemission spectrum of $Cr_{0.62}Te$ also confirmed the existence of short-range FM interaction above T_c [24]. Here the extension from $d=2$ to $d=3$ passing through T_c indicates that $Cr_{0.62}Te$ features quasi-two-dimensional character of chemical bonds and non-negligible exchange interaction along the c axis through the Cr deficient layers; the $n=1$ generally implies uniaxial or Ising-like magnetic interaction. In addition,

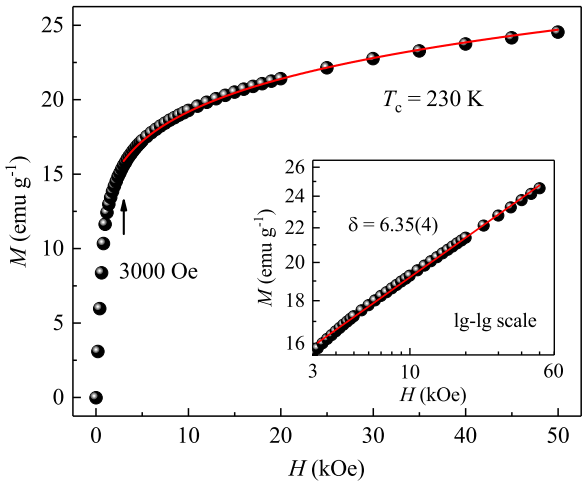

FIG. 8. Isotherm M vs H plot collected at $T_c=230$ K for $Cr_{0.62}Te$. Inset: the same plot in log-log scale with a solid fitting curve.

it is found that the experimental critical exponent of γ is slightly larger than the theoretical value of 2D short-range interaction, and the value of β lies between the theoretical values of 2D long-range interaction and 3D Ising model, further indicating non-negligible interlayer coupling and strong electron-electron correlation in this material [15,24]. The significant hybridization between Cr $3d$ and Te $5p$ bands and strong electron-correlation effects were also previously observed by photoemission spectroscopy [24], confirming the weak itinerant ferromagnetic character of $Cr_{0.62}Te$.

IV. CONCLUSIONS

In summary, we have made a comprehensive study of the critical region at the PM-FM phase transition in the weak itinerant ferromagnet $Cr_{0.62}Te$. This transition is identified to be second order in nature. The critical exponents β, γ, and δ estimated from various techniques match reasonably well and follow the scaling equation, confirming that the obtained exponents are unambiguous and intrinsic to the material. Above T_c the critical exponent $\gamma=1.81(2)$ is close to the short-range interaction with $\{d:n\}=\{2:1\}$ ($\beta=0.125$, $\gamma=1.75$, and $\delta=15.0$) whereas below T_c the critical exponent $\beta=0.315(7)$ lies between the long-range interaction with $\{d:n\}=\{2:1\}$ ($\beta=0.298$, $\gamma=1.392$, and $\delta=5.67$) and 3D Ising model with $\{d:n\}=\{3:1\}$ ($\beta=0.325$, $\gamma=1.24$, and $\delta=4.82$), in correspondence to different classes on the two sides of the magnetic transition. It suggests a change in the nature of magnetic interaction when crossing the transition point, passing from short-range order to long-range order with exchange interaction extending from two to three dimensions on cooling through T_c. Furthermore, with the rapid development in the field of 2D materials, we expect our experimental work to stimulate broad interest in reducing bulk $Cr_{0.62}Te$ to monolayer sheets and possible spintronic application.

ACKNOWLEDGMENTS

This work was supported by the US Department of Energy, Office of Basic Energy Sciences as part of the Computational Material Science Program.

[1] A. K. Geim and I. V. Grigorieva, Nature (London) **499**, 419 (2013).

[2] M. Chhowalla, H. S. Shin, G. Eda, L. J. Li, K. P. Loh, and H. Zhang, Nat. Chem. **5**, 263 (2013).

[3] J. Hu and R. Wu, Nano Lett. **14**, 1853 (2014).

[4] G. R. Bhimanapati, Z. Lin, V. Meunier, Y. Jung, J. Cha, S. Das, D. Xiao, Y. Son, M. S. Strano, V. R. Cooper, L. B. Liang, S. G. Louie, E. Ringe, W. Zhou, S. S. Kim, R. R. Naik, B. G. Sumpter, H. Terrones, F. N. Xia, Y. L. Wang, J. Zhu, D. Akinwande, N. Alem, H. A. Schuller, R. E. Schaak, M. Terrones, and J. A. Robinson, ACS Nano **9**, 11509 (2015).

[5] N. Sivadas, M. W. Daniels, R. H. Swendsen, S. Okamoto, and D. Xiao, Phys. Rev. B **91**, 235425 (2015).

[6] H. L. Zhuang, Y. Xie, P. R. C. Kent, and P. Ganesh, Phys. Rev. B **92**, 035407 (2015).

[7] G. T. Lin, H. L. Zhuang, X. Luo, B. J. Liu, F. C. Chen, J. Yan, Y. Sun, J. Zhou, W. J. Lu, P. Tong, Z. G. Sheng, Z. Qu, W. H. Song, X. B. Zhu, and Y. P. Sun, Phys. Rev. B **95**, 245212 (2017).

[8] L. D. Casto, A. J. Clune, M. O. Yokosuk, J. L. Musfeldt, T. J. Williams, H. L. Zhuang, M. W. Lin, K. Xiao, R. G. Hennig, B. C. Sales, J. Q. Yan, and D. Mandrus, APL Mater. **3**, 041515 (2015).

[9] M. W. Lin, H. L. Zhuang, J. Q. Yan, T. Z. Ward, A. A. Puretzky, C. M. Rouleau, Z. Gai, L. B. Liang, V. Meunier, B. G. Sumpter, P. Ganesh, P. R. C. Kent, D. B. Geohegan, D. G. Mandrus, and K. Xiao, J. Mater. Chem. C **4**, 315 (2016).

[10] X. Zhang, Y. L. Zhao, Q. Song, S. Jia, J. Shi, and W. Han, Jpn. J. Appl. Phys. **55**, 033001 (2016).

[11] H. Ipser, K. L. Komarek, and K. O. Klepp, J. Less-Common Met. **92**, 265 (1983).

[12] G. B. Street, E. Sawatzky, and K. Lee, J. Phys. Chem. Solids **34**, 1453 (1973).

[13] T. Hamasaki and T. Hashimoto, Solid State Commun. **16**, 895 (1975).

[14] M. Akram and F. M. Nazar, J. Mater. Sci. **18**, 423 (1983).

[15] K. Lukoschus, S. Kraschinski, C. Näther, W. Bensch, and R. K. Kremer, J. Solid State Chem. **177**, 951 (2004).

[16] Z. L. Huang, W. Bensch, S. Mankovsky, S. Polesya, H. Ebert, and R. K. Kremer, J. Solid State Chem. **179**, 2067 (2006).

[17] Z. L. Huang, W. Kockelmann, M. Telling, and W. Bensch, Solid State Sci. **10**, 1099 (2008).

[18] M. Chevreton, M. Murat, and C. Eyraud, J. Phys. **24**, 443 (1963).

[19] Y. Adachi, M. Yuzuri, T. Kaneko, and S. Abe, J. Magn. Magn. Mater. **104-107**, 887 (1992).

[20] Y. B. Li, E. Brück, O. Tegus, Y. Q. Zhang, W. J. Feng, N. K. Sun, D. Li, J. Li, T. J. Gortenmulder, Y. K. Huang, and Z. D. Zhang, J. Alloys Compd. **461**, 21 (2008).

[21] M. Yuzuri and Y. Nakamura, J. Phys. Soc. Jpn. **19**, 1350 (1964).

[22] P. Vaqueiro, A. V. Powell, A. I. Coldea, C. A. Steer, I. M. Marshall, S. J. Blundell, J. Singleton, and T. Ohtani, Phys. Rev. B **64**, 132402 (2001).

[23] A. F. Andresen, Acta Chem. Scand. **24**, 3495 (1970).

[24] K. Shimada, T. Saitoh, H. Namatame, A. Fujimori, S. Ishida, S. Asano, M. Matoba, and S. Anzai, Phys. Rev. B **53**, 7673 (1996).

[25] W. Bensch, O. Helmer, and C. Näther, Mater. Res. Bull. **32**, 305 (1997).

[26] E. P. Wohlfarth, J. Magn. Magn. Mater. **7**, 113 (1978).

[27] T. Moriya, J. Magn. Magn. Mater. **14**, 1 (1979).

[28] A. Arrott, Phys. Rev. **108**, 1394 (1957).

[29] S. K. Banerjee, Phys. Lett. **12**, 16 (1964).

[30] A. Arrott and J. Noakes, Phys. Rev. Lett. **19**, 786 (1967).

[31] H. E. Stanley, *Introduction to Phase Transitions and Critical Phenomena* (Oxford University Press, London, 1971).

[32] M. E. Fisher, Rep. Prog. Phys. **30**, 615 (1967).

[33] L. Zhang, H. Han, M. Ge, H. F. Du, C. M. Jin, W. S. Wei, J. Y. Fan, C. J. Zhang, L. Pi, and Y. H. Zhang, Sci. Rep. **6**, 22397 (2016).

[34] A. K. Pramanik and A. Banerjee, Phys. Rev. B **79**, 214426 (2009).

[35] J. S. Kouvel and M. E. Fisher, Phys. Rev. **136**, A1626 (1964).

[36] L. P. Kadanoff, Physics **2**, 263 (1966).

[37] M. E. Fisher, S. K. Ma, and B. G. Nickel, Phys. Rev. Lett. **29**, 917 (1972).

[38] S. Kaul, J. Magn. Magn. Mater. **53**, 5 (1985).

[39] K. Huang, *Statistical Mechanics*, 2nd ed. (Wiley, New York, 1987).

[40] J. C. LeGuillou and J. Zinn-Justin, Phys. Rev. B **21**, 3976 (1980).

[41] S. F. Fischer, S. N. Kaul, and H. Kronmuller, Phys. Rev. B **65**, 064443 (2002).